

Water renewal in semi-enclosed basins: A high resolution Lagrangian approach with application to the Bay of Algeciras, Strait of Gibraltar

Simone Sammartino ^{1*}, José C. Sánchez-Garrido,¹ Cristina Naranjo ¹, Jesús García Lafuente ¹,
Pablo Rodríguez Rubio,² Marcos Sotillo³

¹Physical Oceanography Group, University of Málaga, Málaga, Spain

²Bay of Algeciras Port Authority, Algeciras, Spain

³Puertos del Estado, Madrid, Spain

Abstract

Lagrangian experiments of particle tracking were carried out in the semi-enclosed Bay of Algeciras attached to the Strait of Gibraltar in order to investigate the flushing patterns. A high resolution three-domain-nested hydrodynamic model provided the velocity fields from a 61-d hindcast, with the aim of analyzing the flushing efficiency of eight different docks under a variety of external conditions, namely, tide phase and strength, and winds. The tracking algorithm was specifically developed to exploit the high spatial resolution of the model that reproduces the local dynamics accurately. Winds are the dominant agent, with westerlies featuring *e*-folding times one order of magnitude lower than easterlies. Fortnightly tidal modulation causes a counter-intuitive effect, with spring tides promoting higher accumulation of particles inside the docks and higher *e*-folding times than neap tides. Additionally to high resolution details on the flushing patterns of the Algeciras Port, the model also confirms the Bay as a potential feeder of floating tracers for the nearby Alboran Sea. The proposed approach is easily scalable and exportable to other similar locations worldwide.

The Bay of Algeciras is a densely populated and industrially exploited inlet located at the eastern margin of the Strait of Gibraltar (Fig. 1). The population of the area surrounding the Bay (almost 300,000 residents) generate strong anthropic pressure and the industries located over or nearby the inner coast represent a persistent environmental risk. The main port of the Bay located on the west coast (Fig. 1c), is at first place in the Mediterranean Sea in terms of total throughput (Port of Algeciras Bay 2016), leading the major traffic load from Europe to Africa and from Europe to the rest of the oversea countries. The massive shipping and bunkering together with the harsh weather conditions that often lash the zone boost the environmental hazard, which motivates the need of a deep understanding of the small-scale dynamics of the Bay and the role played by the Port structures in case of oil spill or other surface soiling.

The Bay of around 9×11 km opens southward at the eastern end of the Strait of Gibraltar (Fig. 1a,b), where the

Atlantic jet (AJ hereinafter) starts spreading into the Alboran Sea. After the pioneer study by de Buen (1924), the interest of the scientific community turned to the Strait of Gibraltar itself, displacing the Bay to the background. During the last decade of the 20th century, it attracted the interest of physicists (e.g., Watson and Robinson 1990) and biologists (e.g., Naranjo et al. 1996 and references therein), but it is only recently that more extensive multidisciplinary studies have been published (Álvarez et al. 2011; Periañez 2012; González et al. 2013; Sammartino et al. 2014; Sánchez Garrido et al. 2014; Chioua et al. 2017). A recurrent concern about the Bay is the chronic degree of pollution caused by the intense activities of the local Port and industries, which has been assessed even higher than the one found in the coast of Galicia in the northwest of the Iberian Peninsula after the Prestige oil spill (Morales-Caselles et al. 2007).

The present work aims at characterizing the renewal patterns of this sensitive Bay paying special attention to the fine scale dynamics of the Port structures and their response to different external forcing that could affect their renewal efficiency (i.e., wind, tides). The method proposed employs virtual Lagrangian drifters and a tracking algorithm specifically adapted to reproduce faithfully the particles fate inside the docks. For this reason, it is applicable to any context in which the small-scale circulation and the interaction of

*Correspondence: ssammartino@ctima.uma.es

Additional Supporting Information may be found in the online version of this article.

This is an open access article under the terms of the Creative Commons Attribution License, which permits use, distribution and reproduction in any medium, provided the original work is properly cited.

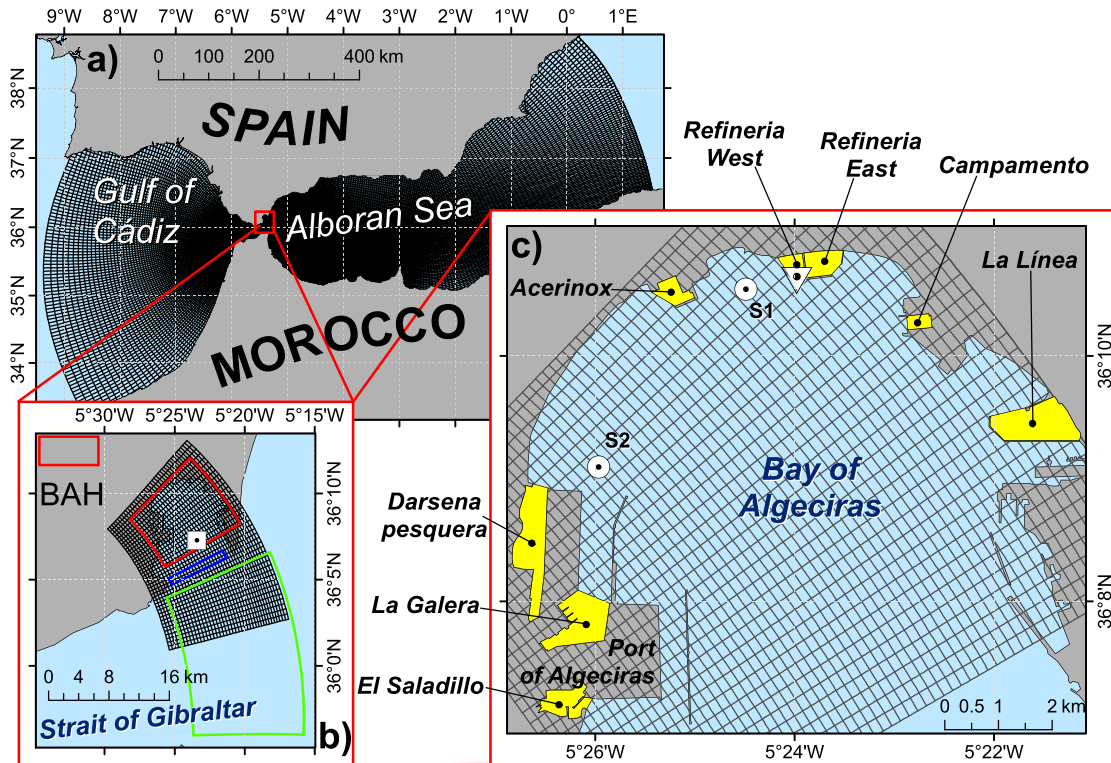


Fig. 1. Maps of the three domains of the model: (a) REG domain, (b) BAM domain with the extent of the BAH domain outlined in red, and the two areas where the latitude of maximum AJ and its mean direction have been computed outlined in green and blue, respectively (see Fig. 5b and “AJ” section for more details). (c) BAH domain with the grid decimated by a factor of 5 for display clearness. The eight docks analyzed in the study are also displayed and labeled. The white square in panel (b) indicates the point at which the wind series illustrated in Fig. 5a is extracted, and the white circles and triangle in panel (c) indicate the locations of the moorings S1 and S2 used for model validation and the tide gauge of the Bay of Algeciras, respectively.

current with the solid boundaries is of fundamental concern (ports, lagoons, channels, etc.). The approach presented is based on two-dimensional (surface) velocity fields and is aimed at modeling the trajectories of particles floating at the surface, especially applicable to the dispersion of surface debris or other floating contaminants.

The hydrodynamic model

This study makes use of three nested numerical models, all them based on the MIT general circulation model (Marshall et al. 1997). The same code has been previously used in this area (Sánchez Garrido et al. 2013, 2014; Sammartino et al. 2014) and we refer to these works for details on model setup. All models use curvilinear grids of variable resolution, which is more visible in the largest domain (REG from REGional model hereinafter, see Fig. 1a). It reaches the maximum resolution inside the Strait of Gibraltar (~ 600 m) and features 46 unevenly distributed z-levels in the vertical. The second domain (BAM, from Bay of Algeciras Medium-resolution, Fig. 1b) covers the Bay of Algeciras and stretches seaward to half the width of the Strait. The downscaling ratio over REG is 1 : 4, which gives a resolution of ~ 150 m,

and the number of z-levels is 35, which also gives higher vertical resolution than REG because of the much lower maximum depth of BAM. The third domain (BAH, from Bay of Algeciras High-resolution, Fig. 1c) nests to BAM with a downscaling ratio of 1 : 5, which implies spatial resolution of ~ 30 m (Fig. 1c), small enough to resolve the civil structures of the Port. It has the same number of z-levels as BAM (35) but higher vertical resolution for the same reasons explained above.

The parent domain REG is forced by the Copernicus Marine Iberian Biscay Irish (IBI) Ocean Analysis and Forecasting system, CMEMS-IBI hereinafter, (Sotillo et al. 2015). It provides the baroclinic fields of temperature, salinity, and horizontal velocity prescribed as open boundary conditions of REG. The storm surge operational NIVMAR model (Fanjul et al. 2001) gives a barotropic correction for the normal velocity at the REG boundaries in order to include the effect of the atmospheric pressure over the Mediterranean basin on the water exchange through the Strait of Gibraltar (García Lafuente et al. 2002). The Spanish Meteorological Agency forecast service based on the HIRLAM model applications (Cats and Wolters 1996; Navascués et al. 2013) provides the atmospheric forcing (wind stress, shortwave and longwave

Table 1. Harmonic constants of M_2 and S_2 constituents for observations (OBS.) vs. model outputs of the barotropic (vertically averaged) current in mooring S1 (see Fig. 1c). Modeled outputs for both REG and BAH domains have been obtained as the weighted average of the four nearest neighbors of the observation point. Tidal harmonic analysis has been performed following Pawlowicz et al. (2002). Errors refer to 95% confidence intervals. Explained variance indicates the percentage of the raw data variance accounted for by the series reconstructed with the estimated harmonic constants.

		OBS.	REG	BAH
Semi-major axis (cm s^{-1})		2.46 ± 1.04	3.91 ± 0.53	1.88 ± 0.40
		0.63 ± 0.84	1.51 ± 0.56	0.99 ± 0.42
Semi-minor axis (cm s^{-1})		-0.06 ± 0.18	0.64 ± 0.27	0.00 ± 0.11
	M_2	-0.08 ± 0.27	0.28 ± 0.27	-0.01 ± 0.11
Phase (degrees)	S_2	52.9 ± 20.8	-11.8 ± 7.0	-37.5 ± 13.4
		287.2 ± 82.4	44.7 ± 21.1	204.3 ± 23.7
Inclination (degrees)		1.3 ± 4.3	-20.2 ± 4.5	2.5 ± 3.0
		15.9 ± 20.8	160.1 ± 10.4	3.4 ± 6.2
Explained variance (%)		10	62	20

surface radiation, precipitation, air humidity, and temperature), while the tidal barotropic velocity computed from the harmonic constants derived by LEGOS-POC/CLS models (Carrère and Lyard 2003) is imposed at the boundaries.

Model validation

The REG model has been already validated at tidal (Sammartino et al. 2014) and subinertial timescales (Sánchez Garrido et al. 2014). The operational system SAMPA (<http://sampa-apba.puertos.es/>) maintained by the Spanish National and Bay of Algeciras Port Authorities uses REG as the hydrodynamic model and, within this frame, its outputs have been further validated against different sources of observations (Soto-Navarro et al. 2016; Jordà et al. 2017), including a validation of the surface fields using the Lagrangian trajectories of a set of surface drifters released in the Strait area (Sotillo et al. 2016).

This work addresses in particular the capability of the model to resolve the local-scale circulation in the nested domains of increased resolution, and therefore it focuses on the comparison of REG and BAH outputs with new sets of observations in order to assess the improvements achieved. To this aim, in agreement with the needs of the local Port Authority to characterize the water column dynamics in the proximity of their port facilities, two simultaneous shallow moorings (S1 and S2, see Fig. 1c) were deployed at approximately 30 m depth in the inner zone of the Bay from December 2015 to January 2016. The moorings were equipped with a Nortek AWAC 600 kHz up-looking Acoustic Doppler Current Profiler (ADCP) clamped to a tripod on the seafloor. Both of them returned very similar results in terms of model validation and only results based on S1 mooring are presented here. Table 1 shows the harmonic constants of the barotropic (vertically averaged) current for M_2 and S_2 constituents from the observations along with the outputs of REG and BAH domains.

For these prevailing semidiurnal constituents, BAH outputs agree with observations better than REG in amplitude and in orientation of the tidal ellipses, which are correctly aligned along the W-E direction (Sammartino et al. 2014). Only the phase of M_2 shows a slightly better agreement with the observations in REG than in BAH. Interestingly, the low percentage of explained variance by tidal currents in the observations is quite similar to the one in BAH, whereas REG predicts an unrealistically large amount of explained variance, suggesting a rather deterministic contribution in the total current that is not confirmed by observations.

The analysis of the baroclinic velocity (Fig. 2) is coherent with the previous results because the baroclinicity of the water column is expectedly weak in such a shallow location. Almost all the harmonic constants of the M_2 constituent (phase is again the exception) show better agreement for BAH than for REG simulations. Despite their weakness, amplitudes are very satisfactorily matched by BAH and the ellipses inclinations fall within their respective confidence intervals.

In order to assess the reliability of solutions at subinertial scale, the prevailing zonal component of the current (see ellipse orientation in Fig. 2) has been filtered applying a Godin filter (Godin 1972), and the detided modeled outputs have been compared with observations (Fig. 3). Figure 3 also shows the vertical profiles of maximum correlation coefficients obtained by cross-correlation analysis, as well as their corresponding lags (more details in the caption of the figure). BAH model generally provides much better results than REG, with a vertically averaged maximum correlation with observations of 0.63 at a lag varying from -1 d to $+1$ d, approximately, against the mean maximum value of 0.24 provided by REG model. The short lags observed become negligible if the first week of the series is removed in the cross-correlation analysis, suggesting a slightly longer adjustment time of subinertial scale processes to the model initial

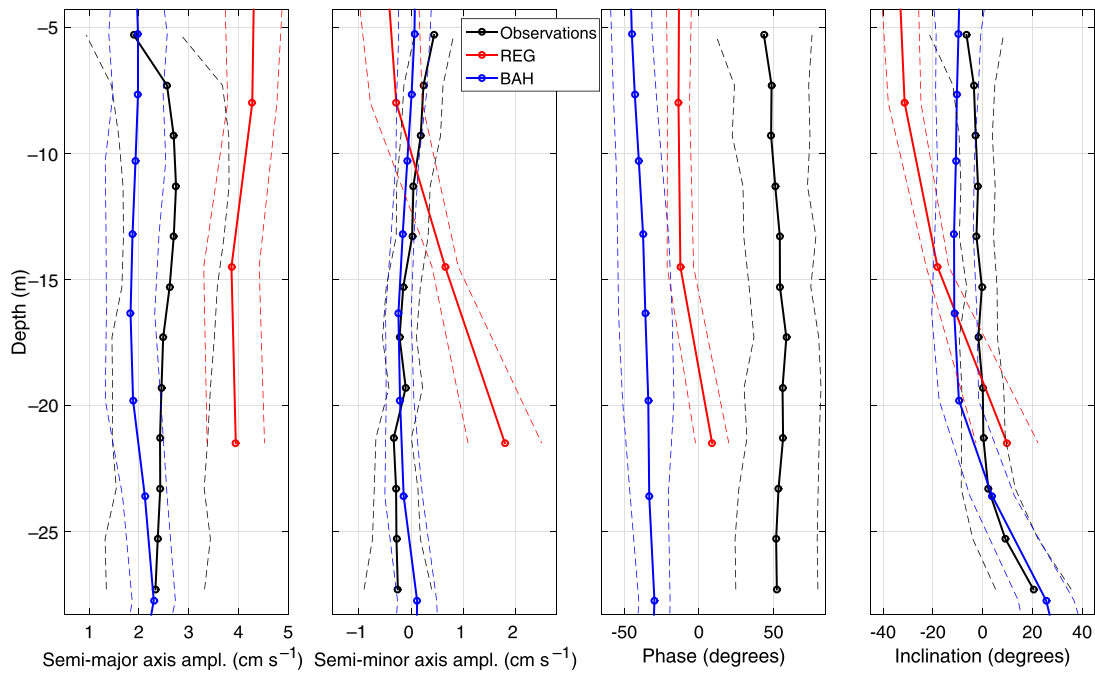


Fig. 2. Vertical profiles of harmonic constants of the M_2 tidal ellipses for REG and BAH modeled outputs and observations collected at mooring S1 (see Fig. 1c). Dashed lines indicate the 95% confidence intervals for each profile.

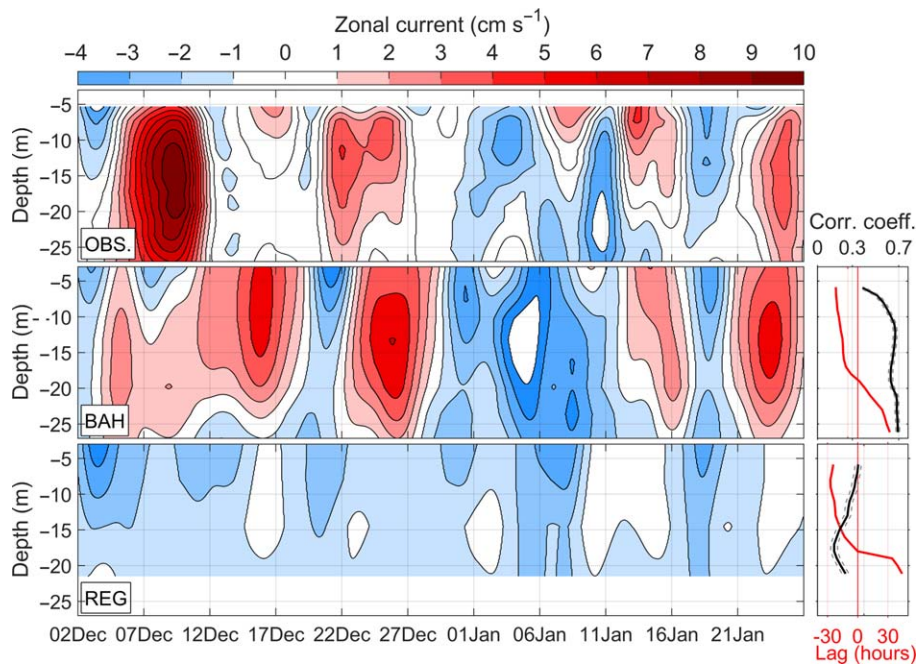


Fig. 3. Detided series of zonal current profiles in S1 location for observed and simulated (BAH, REG) records. Plots of the vertical profiles of maximum correlation coefficient (black line) obtained by cross-correlation analysis of observations vs. BAH (up) and REG (down), with corresponding 95% confidence intervals (gray dotted line), and the corresponding lags (red line) at which these maxima have been found are shown on the right panels. Negative (positive) lags indicate modeled outputs lagging (leading) observations. The vertical red line indicates zero-lag.

conditions. Whatever the case, results reveal the improved capability of the finer model to resolve the local scale, and give confidence on the use of this domain for a reliable simulation of the inner Bay and Port circulation.

Particle trajectory computation

The algorithm used to compute the particles trajectories is an inedited code of the Runge-Kutta 4th order advection scheme (RK4) specifically adapted to our model geometry. The spatial interpolation of the surface current speed at the particle position is made directly on the native Arakawa-C curvilinear grid of the model. The selection of the optimal intervals for model outputs recording and RK4 algorithm iteration is explained in Supporting Information Appendix A.

In order to address processes of scale smaller than the grid model (e.g., turbulence), a stochastic contribution (random walk) has been added to the deterministic advection term. The algorithm prescribes the position of the particle at a forward time as:

$$x_i(t_j + \Delta t) = x_i(t_j) + \bar{U}_i(t_j, x) \Delta t + \sqrt{2} r_i R \quad (1)$$

where x_i , $i=[1,2]$, is the i -th coordinate of the particle, $\bar{U}_i(t_j, x)$ is the mean surface velocity in the i -th direction at time t_j and position x , r_i is the root mean square of the velocity in the i -th direction computed on the two model outputs corresponding to time steps before and after t_j , and R is a white Gaussian noise, with unit variance (LaCasce 2008). Since the model outputs are time-averaged velocities every 15 min (see Supporting Information Appendix A), they have been identified with term $\bar{U}_i(t_j, x)$ in Eq. 1. The first two terms in the right hand side of Eq. 1 are computed with the RK4 method, whereas the stochastic term is added subsequently. At each iteration, $\bar{U}_i(t_j, x)$ is taken from the finest domain output: BAH if it is inside BAH domain, BAM if it is outside of BAH but inside of BAM domain, and REG otherwise.

Interaction particle-solid boundaries

Lagrangian particle tracking algorithms in the open ocean use to assign a fixed position (the last valid) to tracers that hit land (e.g., Fredj et al. 2016). In our case, the interaction of the particles with the solid boundaries is of relevance and a stagnant position for a particle that hits the land is neither suitable nor realistic to simulate their evolution inside the Port structures. More realistically, the particle is shacked by swell or turbulence and eventually drifted away by the long-shore component of the current, for which we apply the following correction to the advection term in Eq. 1.

Whenever the algorithm prescribes a particle trajectory crossing a solid boundary, we decompose the interpolated velocity vector at the particle position in long-shore (A) and (minus, seaward) cross-shore (B) components (see sketch in Fig. 4).

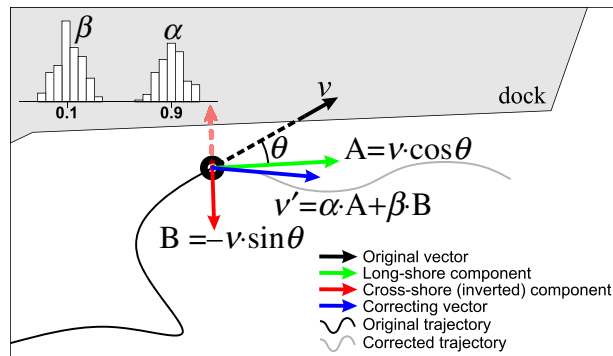


Fig. 4. Sketch of the trajectory correction applied in case of solid boundary crossing.

We compute a weighted average of both components (weights α and β come from two random Gaussian distributions with means 0.9 and 0.1, respectively, and 0.1 variance, normalized to sum unity to preserve the modulus of the original velocity), assigning the highest (lowest) weight to the long-shore (cross-shore) component. The resulting v' velocity advects the particle along the solid boundary and, at the same time, gives it some chances for seaward drift. In other words, the algorithm allows it to detach from the inner boundaries and be washed away, instead of remaining stagnant.

Simulated dataset

The model has been run by importing initial and boundary conditions in the parent REG domain from the CMEMS-IBI model (“The hydrodynamic model” section). Under this forcing, the system reaches a stable solution in 4–5 d approximately so that a spin-up time of a week has been applied prior to the release of particles.

We run a 61-d hindcast of the three domains during December 2015–January 2016 (the same period of available observations used for validation, see “Model validation” section), and identified different combinations of wind and tide conditions in order to have a variety of situations for carrying out the tracking experiments. The explored scenarios arise from the combination of three wind conditions (easterlies or Levante, westerlies or Poniente, and calm), two tidal phases (flood and ebb), and two tidal intensities (spring and neap tide). The cases of wind calm were only addressed for neap tide. The possible combinations sum up 10 different scenarios that can be identified in Fig. 5 where the two components of winds and the sea level during the simulated period are displayed. The figure also shows the position and direction of the AJ, the surface current entering the Mediterranean through the Strait of Gibraltar, whose influence has been assessed in a different set of experiments that will be discussed later on. The analyzed period, yet not exhaustive,

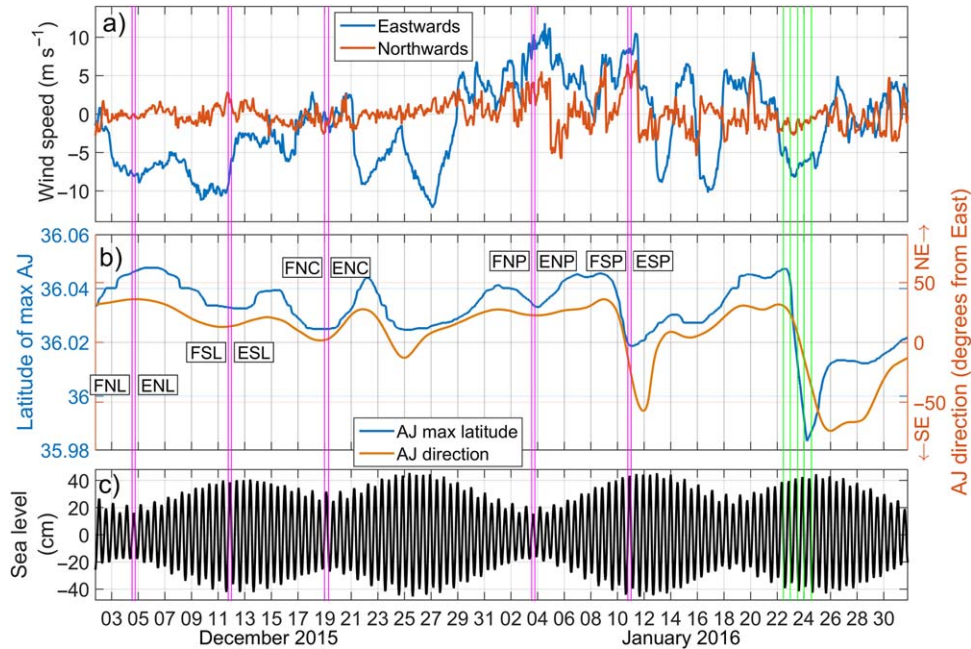


Fig. 5. Panel (a): wind eastward and northward components extracted from the HIRLAM model in the point displayed in Fig. 1b. Panel (b): latitude of the maximum velocity and mean direction of the AJ estimated within the regions highlighted in Fig. 1b. The labels NE (northeastward) and SE (southeastward) help to interpret the AJ direction. Current velocity has been previously detided by applying a Godin filter (Godin 1972). Panel (c): sea level at Algeciras tide gauge (white triangle in Fig. 1c). The times of particles release for the scenarios analyzed in the text are indicated by magenta vertical lines, and labeled with a three-letter code according to: Flood/Ebb (tide phase), Spring/Neap (tide strength) and Levante/Poniente/Calm (wind direction). The green lines indicate the release times of the experiments carried out to assess the effect of the AJ on the renewal efficiency of the Bay.

gathers a high variability of the forcings involved and allows for a proper characterization of the Port dynamics in a wide range of conditions.

The particle tracking experiments corresponding to the aforementioned scenarios have been performed on eight docks of special interest (yellow polygons in Fig. 1c referred to as UGAPs hereinafter for the Spanish definition of Port Water Management Unit), which amounts up to 80 experiments. In each of them, a maximum of 2400 particles was randomly released inside the UGAP (*see* Supporting Information Appendix A), and the particles trajectories were tracked for 10 d. A further set of 10 experiments have been conducted to evaluate the effect of the variability of the AJ (green lines in Fig. 5) on two representative docks. In order to assess the intrinsic variability and statistical confidence of the indicators used in the study, a series of repeated runs of different experiments have been performed. Finally, the whole Bay of Algeciras has been studied under westerly regime during the ebb phase of a spring tide (ESP case, *see* Fig. 5), which are the most favorable conditions for an effective surface ventilation according to Sammartino et al. (2014) and Sánchez Garrido et al. (2014). In this experiment, more than 6000 particles have been released and their trajectories tracked for 15 d.

Flushing time and residence time map

One metric widely employed in the analysis of water renewal of semi-enclosed basins is the bulk time scale known as flushing time. Several definitions of flushing time can be found in literature (Zimmerman 1976; Takeoka 1984; Mønsen et al. 2002). It is strictly defined as the ratio of volume of water to the volume transport across the basin open boundaries (Zimmerman 1976). However, in the hypothesis of the continuous stirring tank reactor (Mønsen et al. 2002; Rayson et al. 2016) where any insertion of mass in the domain is assumed to be instantaneously and homogeneously mixed, it can be estimated from the tracking of mass concentration over the time. In a Lagrangian framework, such concentration is represented by particles abundance inside the dock, varying according to trajectories evolution, and can be least-squares fitted by an exponential function as follows:

$$C(t) = 100e^{-t/a} \quad (2)$$

Here $C(t)$ is the percentage of particle at time t and a is the e -folding time, the time required to reduce the number of particle inside the study area by a factor of e . The e -folding flushing time, as defined by Mønsen et al. (2002), is widely used in environmental science (Sánchez Garrido et al. 2014;

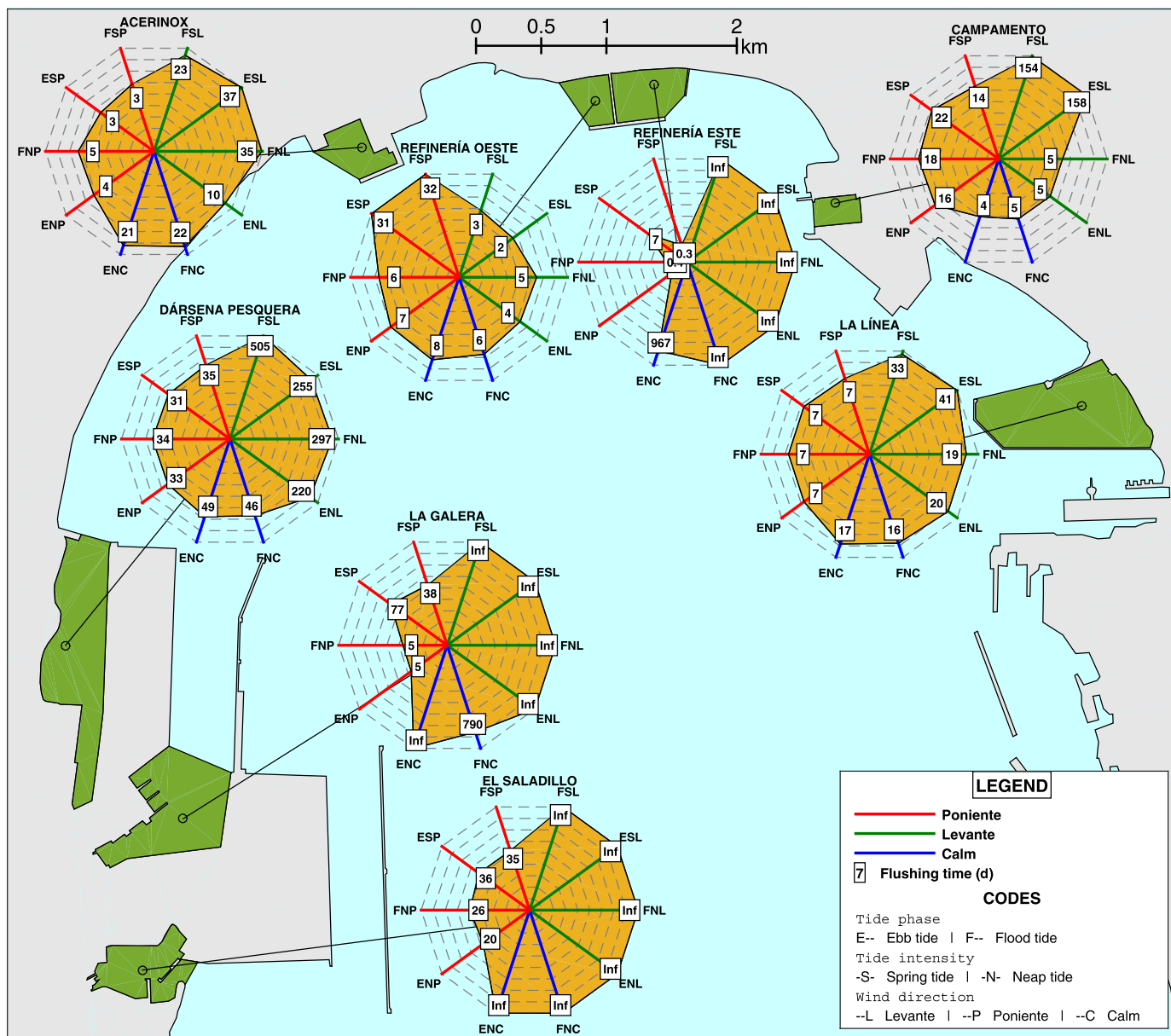


Fig. 6. Radar charts of the e -folding times of the UGAPs analyzed under all the possible combinations of initial conditions summarized in “Simulated dataset” section. Westerlies (Poniente) and easterlies (Levante) cases are represented in the left and right half of the radar charts, respectively, following the direction of provenience of the winds. Calm cases (blue lines) are on the bottom. Wind and tide labeling is explained in the legend. The value *Inf* indicates e -folding times greater than 1000 d.

Rayson et al. 2016; Viero and Defina 2016 and references therein) and it is actually recommended by the Bay of Algeciras Port Authority (Juanes et al. 2013).

Flushing time is a bulk time scale and, albeit providing a global characterization of the flushing efficiency of the basin, it does not allow for a spatial analysis of the inlet dynamics. Residence time is defined as the time a single particle takes to reach the outlet from the inlet (Zimmerman 1976; Takeoka 1984; Tartinville et al. 1997). Although it can be integrated over the volume of the inlet, or portions of it

(Pawlowicz et al. 2007), it should be considered as a spatially dependent time scale because it greatly depends on the particle position and the time of release (Monsen et al. 2002; Rayson et al. 2016). Here, we propose a residence time map calculated as the maximum time spent by any particle inside each element of a regular grid in which the UGAP is discretized (grid resolution is 30 m, according to BAH resolution). These maps reflect the main circulation patterns of the UGAPs: the highest times are typically found along the inner boundaries where the currents are weaker, or along the edges

of the cells of circulation occurring inside the UGAPs, while the lowest values are detected at the dock entrance or at the interior of those cells. For each experiment, we then provide both the bulk e -folding flushing time and the spatially varying residence time map.

Results

Figure 6 displays the flushing times of all the UGAPs (Fig. 1c) under all the possible combinations summarized in “Simulated dataset” section. Based on a series of repeated replicas of 15 experiments selected among those that provide

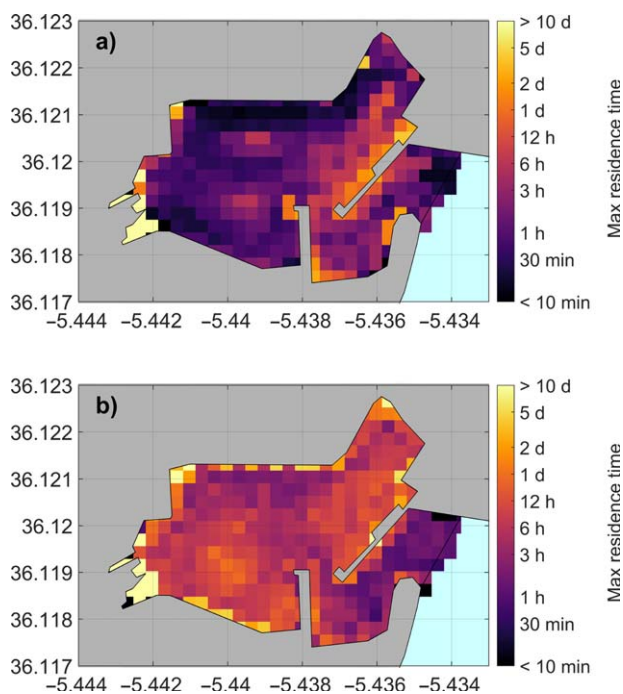


Fig. 7. Residence time maps computed for the UGAP “El Saladillo” in ebb, neap tide and under westerlies (a) and calm (b).

reasonable flushing times, we have estimated a mean statistical confidence of $\sim 4\%$ (ratio of 95% confidence intervals to the mean flushing times for each experiment), which account for the uncertainties of the stochastic term of Eq. 1 and the random initialization of particles position. The percentage increases to $\sim 5\%$ if the analysis includes four more replicas in which the release time changes from 30 min before to 30 min after.

Wind

A clear bias to flushing times driven by winds emerges from the radar charts in Fig. 6: most of the UGAPs present flushing times one order of magnitude less on average under westerlies than under easterlies. Those oriented eastward, such as “La Galera,” “El Saladillo,” and “Refinería Este,” show flushing times greater than 1000 d under easterlies (set as Inf in Fig. 6): they are rather enclosed docks with limited circulation, for which only favorable winds from the West and Southwest give chances for flushing. Conversely, easterlies accumulate water inside the docks blocking any possibility of water renewal.

Figure 7 shows the effect of wind on the residence time maps. Westerlies (Fig. 7a) wash water out of the UGAP “El Saladillo,” piling it up at the pier located at the main entrance: residence time inside most of the UGAP is less than few hours. Rather different is the situation under no wind conditions, when residence times are $O(1\text{ d})$ inside the dock and longer along the innermost boundaries (Fig. 7b). The corresponding flushing times are 20 d and Inf for westerlies (ENP case) and calm conditions (ENC case), respectively (see Fig. 6). This UGAP is quite efficiently flushed by westerlies, but the residence time map reveals that the transverse pier represents a strong barrier for a much more efficient ventilation of the dock.

Another clear example is the UGAP “La Línea”: here westerlies (blue lines in Fig. 8) remove 40% of particles within the first 2 d, a small fraction of them (less than 10%)

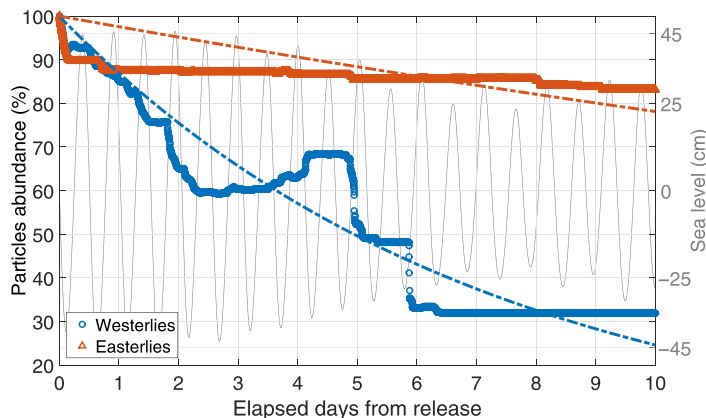


Fig. 8. Observed particles abundance in the UGAP “La Línea” in ebb, spring tide and westerlies (blue circles) and easterlies (red triangles). The corresponding fits of Eq. 2 are also shown in dot-dashed lines.

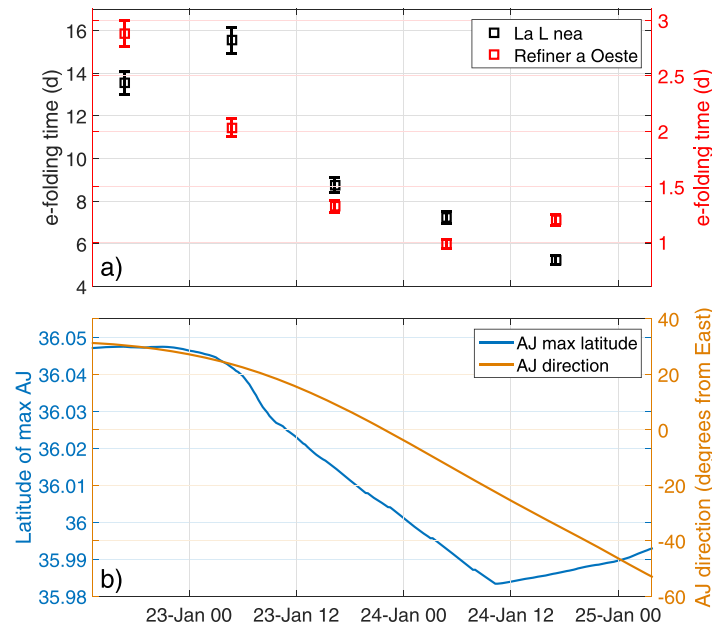


Fig. 9. Panel (a): e -folding times obtained for the UGAPs “La Línea” (black squares, left axis) and “Refinería Oeste” (red squares, right axis) under ebb, spring, and easterlies conditions corresponding to the experiments highlighted with green lines in Fig. 5. The 95% confidence intervals are indicated by the bars. Notice the different scales of the two vertical axes. Panel (b): zoom of Fig. 5b showing the changes of latitude of maximum and mean direction of the AJ during the dates indicated by the green lines in that figure.

recirculate inside the dock during the fourth day, and eventually another 40% is quickly driven away within just 1 d more. From day 6 onward, the particles inside the dock keep circulating sluggishly around the less energetic inner margins, and the curve holds constant.

On the other hand, under easterlies (red lines in Fig. 8), while a small fraction ($\sim 10\%$) of particles in the proximity of the entrance of the dock leaves it within the first 4 h (ebb current), a cyclonic cell forced by winds and propitiated by the geometry of the dock traps the rest of particles afterward, which only very occasionally reach the exit and escape out. The corresponding e -folding times are 7 d and 41 d, for westerlies and easterlies, respectively (see ESP and ESL cases in Fig. 6).

An exhaustive analysis of the effect of the wind intensity alone for a given wind direction cannot be properly performed with our set of realistic scenarios. Depending on the dock selected, the choice of a different release time with different wind intensity cannot provide definitive conclusions because of the concomitant contribution of other factors (tide strength and phase) that can mask the potential effect of wind strength variability. To this aim, a series of artificial scenarios should have been defined, but it is out of the scope of the present study.

Tide

The effect of tides in the renewal capacity of the UGAPs is subtler, yet important. Spring tides increase the amplitude of the tidal excursions and enhance the in-out swinging of the

particles. Intuitively, more effective ventilation is expected under spring tide, but the results do not confirm this intuition. For instance, the two flood tide cases FSL and FNL under easterlies of the UGAP “Campamento” (see Fig. 6) present e -folding times of 154 d and 5 d, respectively. Flood current suction particles out of the dock in both cases, but the strength of the spring tide pushes them back during the next ebb cycle, favoring the accumulation inside the dock. The particles progressively move to the inner area where currents are weaker and end up recirculating mostly inside the UGAP. In neap tide, on the contrary, although the first thrust of the flood current is weaker, the subsequent ebb is weaker too and it does not push particles completely inside the dock, which results in an overall more effective ventilation.

The impact of the tide phase on flushing times is even weaker. Ebb tide tends to ventilate water out of the Bay and favor its renewal (Sammartino et al. 2014). At local scale, the renewal depends on the very location and orientation of the dock. Whatever the case, tidal currents affect the particles trajectories mainly during the first 6 h of simulation and, since the e -folding times are computed over a time horizon of 10 d, their influence fades out progressively as the experiments go ahead. Few exceptions exist, as the case of the UGAP “La Galera” under westerlies/spring tide conditions: here flood current enters the Bay suctioning particles toward the open boundary of the dock and favoring the action of the wind, while ebb flow, yet marginal, hampers the wind effect. The corresponding e -folding times are 38 d and 77 d for flood (FSP) and ebb (ESP) cases, respectively (Fig. 6).

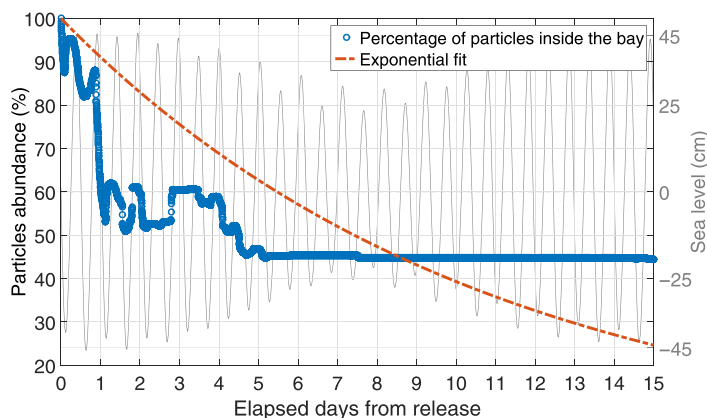


Fig. 10. Observed particles abundance in the whole Bay. Fitted Eq. 2 is also shown.

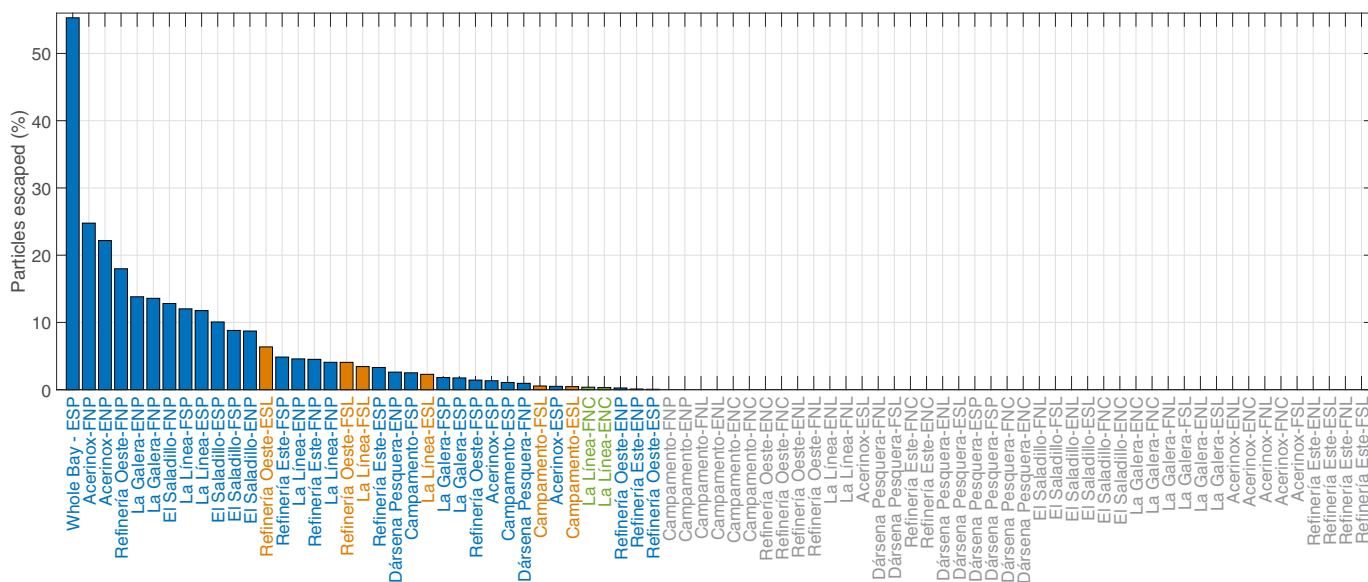


Fig. 11. Percentage of particles escaped out of the Bay for all the experiments run. Blue, orange, and green bars indicate experiments run under westerlies, easterlies, and calm, respectively. The same color code is used for labels. Experiments in which no particles leave the Bay are labeled in gray.

AJ

The AJ is known to be modulated in amplitude and direction at different time scales (Garrett et al. 1989; García Lafuente et al. 1998; Sarhan et al. 2000; Vargas-Yáñez et al. 2002). Although the atmospheric pressure gradient between the western Mediterranean and the Gulf of Cádiz is the main source of subinertial modulation of the inflow and of the own Jet (García Lafuente et al. 2002b; Sánchez Garrido et al. 2013), local wind has also been proven to determine marked deflections of the very surface current, especially ahead of the Bay entrance (García Lafuente et al. 2002a; Sánchez Garrido et al. 2014; Chioua et al. 2017): westerly (easterlies) winds seem to favor an intensification (weakening) of the AJ and its deflection southward (northward).

Whatever the cause of the AJ fluctuations, it is clear that the intensity and especially the position of this swift current flowing close to the entrance of the Bay has to influence its renewal efficiency. Figure 9 shows the results of two series of experiments run in the UGAPs “La Línea” and “Refinería Oeste” as examples of docks near and far from the Bay entrance, respectively.

The experiments have been run for five ebb tides during the strongest AJ variation observed in the time series depicted in Fig. 5b. Figure 9b shows that the AJ state changes from flowing mostly east-northeastward close to the Bay mouth to shift to the south and flow southeastward in less than 2 d. In the first situation, the AJ would hamper the outward current from the Bay and reduce the ventilation of the

surface layer, a constraint that is not met in the second situation. The clear diminution of the flushing e -folding times of both docks with time (down to $\sim 65\%$ of the initial value, see Fig. 9a) matches the evolution of the AJ and confirms this hypothesis.

Whole Bay renewal performance

The experiment made for the whole Bay of Algeciras offers a global view of the renewal efficiency of the inlet that combines the open area dynamics of the center of the Bay, where the interaction with the Port structure is not an issue, and the finer scale flushing mechanisms of its peripheral docks. Figure 10 shows the evolution of particles abundance through the 15 d of simulation.

The tidally driven circulation in the Bay is clearly reflected by the marked semidiurnal oscillations of the abundance curve: they are observable during the first 5 d, with higher losses occurring during ebb tides. Animation V1* helps interpret the origin of the drops of the first three ebb cycles, when a large number of particles leaves the Bay along the flanks, especially through the eastern one. From day 5 onward, the depletion ceases and the remaining particles follow circulating sluggishly in the peripheral docks. The residual concentration, estimated as the asymptotic trend of the curve at the end of the experiment, is notable ($\sim 45\%$) and the resulting e -folding time is 10.7 d.

Discussions and conclusions

The surface circulation of the Bay of Algeciras is mainly driven by tides and secondarily modulated by winds: Atlantic surface water enters the Bay in the flood tide and flows out in the ebb tide (Sammartino et al. 2014), while westerly (easterly) winds produce a prevailing outward (inward) surface current (Sánchez Garrido et al. 2014). The analysis of the particles trajectories confirms this general scheme, although it depicts more complex patterns arising from the interaction of the general circulation with the Port civil structures. Winds are by far the primary source of variability of the flushing times computed throughout the 80 cases investigated: westerlies tend to drag water out of the Bay by Ekman transport, whereby its effect on each single UGAP depends on the own geometry, size and orientation of the dock. Most of the UGAPs, especially those located on the western flank of the Bay, have e -folding times under westerlies up to one, even two, orders of magnitude lower than under easterlies. Among the experiments that present a significant quantity of particles exported out of the Bay (45% of the total, see Fig. 11), the 78% of them are under westerlies (blue bars), while only 17% are under easterlies (orange

bars), the latter with proportions of particles exported not exceeding the 6% (Fig. 11). Although a higher resolution of the wind forcing in the model would improve the reproducibility of the small-scale dynamics of the docks, their strong dependence on wind direction disclosed by the experiments could possibly be extrapolated to the whole Bay, which would be far better flushed by westerlies.

The effect of the spring-neap tide alternation depends on the spatial scale considered: at Bay scale, the higher the strength of the tide, the higher the total displacement of the particles and, hence, the greater the probability for them to be entrained by the AJ and advected past the Gibraltar Rock into the Alboran Sea, as observed by Sánchez Garrido et al. (2014). Nonetheless, at dock scale the opposite occurs: actually the first six cases of highest percentages of particles exported out of the Bay are in neap tide conditions (and westerlies), with values spanning from 13% to 25% (see x -axis coded labels in Fig. 11).

The e -folding flushing time obtained for the whole Bay experiment under conditions of westerlies and ebb spring tide (which gather the most favorable conditions for an effective ventilation) is 10.7 d. When this result is compared with that obtained by Sánchez Garrido et al. (2014), who used a different method and a nonconservative passive tracer on a coarser domain to obtain flushing times of 3.4 d, we conclude that the increase in the model resolution and especially the inclusion of the Port structures in the domain has great influence on the assessment of the flushing times of the Bay and are behind the disparity of these results. Regardless whether or not winds are more efficient than tides, the presence of docks and piers forces particle recirculation ($\sim 45\%$ as seen in Fig. 10) and impacts the renewal efficiency of the Bay as a whole. The effect of particles withdrawal occurring in the peripheral docks makes that the abundance curve shown in Fig. 10 does not exhibit the smoothed periodic tidal oscillation superimposed to the damping depicted in Fig. 10 of Sánchez Garrido et al. (2014), but it displays a more irregular variability instead.

The Algeciras Bay plays different roles regarding the nearby Alboran Sea. It is a source of nutrients and phytoplankton biomass (Sánchez Garrido et al. 2015), but it also is a time bomb because of the intense shipping and bunkering of the own port, which poses very serious consequences on the local and neighboring ecosystem. Whatever the case, the Bay is a source of matter susceptible to be exported out to the nearby basin, and this work shows that this process is strongly dependent on the scale of the phenomenon (in terms of the Bay dimensions), as well as on the location and on the specific external conditions acting on the system at the moment. The trajectory of the particles and their eventual spreading into the Alboran Sea depend on the combination of several factors, starting with winds if an accident happens in an inner dock where ventilation is dominated by winds, but also on the tides that contribute noticeably to

*Animation V1. Particles trajectories evolution throughout the 15 d of simulation of the whole Bay experiment. https://youtu.be/4_GSoQRuk8w

drive the exchange with the external channel in the center of the Bay, not neglecting the important role of the AJ dynamics in favoring or hampering the Bay ventilation. The satisfactory understanding of this combination of scales and forcings is crucial to work out the complex relationship between the Bay and the nearby basin, and to design and improve protocols to follow by local authorities in case of accident in the Port area.

References

- Álvarez, Ó., C. J. González, R. Mañanes, L. López, M. Bruno, A. Izquierdo, J. Gómez-Enri, and M. Forero. 2011. Analysis of short-period internal waves using wave-induced surface displacement: A three-dimensional model approach in Algeciras Bay and the Strait of Gibraltar. *J. Geophys. Res.* **116**: C12033. doi:10.1029/2011JC007393
- Carrère, L., and F. Lyard. 2003. Modeling the barotropic response of the global ocean to atmospheric wind and pressure forcing—comparisons with observations. *Geophys. Res. Lett.* **30**: 1275. doi:10.1029/2002GL016473
- Cats, G., and L. Wolters. 1996. The Hirlam project [meteorology]. *IEEE Comput. Sci. Eng.* **3**: 4–7. doi:10.1109/99.556505
- Chioua, J., and others. 2017. Water exchange between Algeciras Bay and the Strait of Gibraltar: A study based on HF coastal radar. *Estuar. Coast. Shelf Sci.* **196**: 109–122. doi:10.1016/j.ecss.2017.06.030
- Courant, R., K. Friedrichs, and H. Lewy. 1967. On the partial difference equations of mathematical physics. *IBM J. Res. Dev.* **11**: 215–234. doi:10.1147/rd.112.0215
- de Buen, R. 1924. Avance al estudio oceanográfico de la bahía de Algeciras. *Bol. Pesca I.E.O.* **89**: 1–35.
- Fanjul, E. Á., B. P. Gómez, and I. R. S. Arévalo. 2001. Nivmar: A storm surge forecasting system for Spanish waters. *Sci. Mar.* **65**: 145–154. doi:10.3989/scimar.2001.65s1145
- Fredj, E., D. F. Carlson, Y. Amitai, A. Gozolchiani, and H. Gildor. 2016. The particle tracking and analysis toolbox (PaTATO) for Matlab. *Limnol. Oceanogr.: Methods* **14**: 586–599. doi:10.1002/lom3.10114
- García Lafuente, J., J. Delgado, and F. Criado. 2002a. Inflow interruption by meteorological forcing in the Strait of Gibraltar. *Geophys. Res. Lett.* **29**: 20-1–20-4. doi:10.1029/2002GL015446
- García Lafuente, J., J. Delgado, J. M. Vargas, M. Vargas, F. Plaza, and T. Sarhan. 2002b. Low-frequency variability of the exchanged flows through the Strait of Gibraltar during CANIGO. *Deep-Sea Res. Part II Top. Stud. Oceanogr.* **49**: 4051–4067. doi:10.1016/S0967-0645(02)00142-X
- Garrett, C., J. Akerley, and K. Thompson. 1989. Low-frequency fluctuations in the Strait of Gibraltar from MEDALPFX sea level data. *J. Phys. Oceanogr.* **19**: 1682–1696. doi:10.1175/1520-0485(1989)019<1682:LFFITS>2.0.CO;2
- Godin, G. 1972. *The analysis of tides*. Univ. of Toronto Press.
- González, C. J., Ó. Álvarez, R. Mañanes, A. Izquierdo, M. Bruno, J. J. Gomiz, J. Chioua, and L. López. 2013. Baroclinic M2 tidal circulation in Algeciras Bay and its implications for the water exchange with the Strait of Gibraltar: Observational and 3-D model results. *J. Geophys. Res. Oceans* **118**: 5398–5411. doi:10.1002/jgrc.20404
- Jordà, G., A. Sánchez-Román, and D. Gomis. 2017. Reconstruction of transports through the Strait of Gibraltar from limited observations. *Clim. Dyn.* **48**: 851–865. doi:10.1007/s00382-016-3113-8
- Juanes, J. A., B. Ondiviela, A. G. Gómez, and J. A. Revilla. 2013. Recommendations for maritime works - ROM 5.1-13. Quality of coastal waters in port areas, p. 158. Ministerio de Fomento.
- LaCasce, J. H. 2008. Statistics from Lagrangian observations. *Prog. Oceanogr.* **77**: 1–29. doi:10.1016/j.pocean.2008.02.002
- Lafuente, J. G., N. Cano, M. Vargas, J. P. Rubín, and A. Hernández-Guerra. 1998. Evolution of the Alboran Sea hydrographic structures during July 1993. *Deep-Sea Res. Part I Oceanogr. Res. Pap.* **45**: 39–65. doi:10.1016/S0967-0637(97)00216-1
- Marshall, J., A. Adcroft, C. Hill, L. Perelman, and C. Heisey. 1997. A finite-volume, incompressible Navier Stokes model for studies of the ocean on parallel computers. *J. Geophys. Res. Oceans* **102**: 5753–5766. doi:10.1029/96JC02775
- Monsen, N. E., J. E. Cloern, L. V. Lucas, and S. G. Monismith. 2002. A comment on the use of flushing time, residence time, and age as transport time scales. *Limnol. Oceanogr.* **47**: 1545–1553. doi:10.4319/lo.2002.47.5.1545
- Morales-Caselles, C., J. Kalman, I. Riba, and T. A. DelValls. 2007. Comparing sediment quality in Spanish littoral areas affected by acute (*Prestige*, 2002) and chronic (Bay of Algeciras) oil spills. *Environ. Pollut.* **146**: 233–240. doi:10.1016/j.envpol.2006.04.042
- Naranjo, S. A., J. L. Carballo, and J. C. Garcia-Gomez. 1996. Effects of environmental stress on ascidian populations in Algeciras Bay (southern Spain). Possible marine bioindicators? *Mar. Ecol. Prog. Ser.* **144**: 119–131. doi:10.3354/meps144119
- Navascués, B., and others. 2013. Long-term verification of HIRLAM and ECMWF forecasts over Southern Europe: History and perspectives of Numerical Weather Prediction at AEMET. *Atmos. Res.* **125–126**: 20–33. doi:10.1016/j.atmosres.2013.01.010
- Pawlowicz, R., B. Beardsley, and S. Lentz. 2002. Classical tidal harmonic analysis including error estimates in MATLAB using T_TIDE. *Comput. Geosci.* **28**: 929–937. doi:10.1016/S0098-3004(02)00013-4
- Pawlowicz, R., O. Riche, and M. Halverson. 2007. The circulation and residence time of the strait of Georgia using a

- simple mixing-box approach. *Atmosphere-Ocean* **45**: 173–193. doi:10.3137/ao.450401
- Periáñez, R. 2012. Modelling the environmental behaviour of pollutants in Algeciras Bay (south Spain). *Mar. Pollut. Bull.* **64**: 221–232. doi:10.1016/j.marpolbul.2011.11.030
- Port of Algeciras Bay. 2016. Port of Algeciras handbook 2015–2016, Comport Bahía de Algeciras, Algeciras.
- Rayson, M. D., E. S. Gross, R. D. Hetland, and O. B. Fringer. 2016. Time scales in Galveston Bay: An unsteady estuary. *J. Geophys. Res. Oceans* **121**: 2268–2285. doi:10.1002/2015JC011181
- Sammartino, S., J. García Lafuente, J. C. Sánchez Garrido, F. J. De los Santos, E. Álvarez Fanjul, C. Naranjo, M. Bruno, and C. Calero. 2014. A numerical model analysis of the tidal flows in the Bay of Algeciras, Strait of Gibraltar. *Cont. Shelf Res.* **72**: 34–46. doi:10.1016/j.csr.2013.11.002
- Sánchez Garrido, J. C., G. Sannino, L. Liberti, J. García-Afuente, and L. Pratt. 2011. Numerical modeling of three-dimensional stratified tidal flow over Camarinal Sill, Strait of Gibraltar. *J. Geophys. Res. Oceans* **116**: C12026. doi:10.1029/2011JC007093
- Sánchez Garrido, J. C., J. García Lafuente, E. Álvarez Fanjul, M. G. Sotillo, and F. J. de los Santos. 2013. What does cause the collapse of the Western Alboran Gyre? Results of an operational ocean model. *Prog. Oceanogr.* **116**: 142–153. doi:10.1016/j.pocean.2013.07.002
- Sánchez Garrido, J. C., J. García Lafuente, S. Sammartino, C. Naranjo, F. J. de los Santos, and E. Álvarez Fanjul. 2014. Meteorologically-driven circulation and flushing times of the Bay of Algeciras, Strait of Gibraltar. *Mar. Pollut. Bull.* **80**: 97–106. doi:10.1016/j.marpolbul.2014.01.036
- Sánchez Garrido, J. C., C. Naranjo, D. Macías, J. García-Lafuente, and T. Oguz. 2015. Modeling the impact of tidal flows on the biological productivity of the Alboran Sea. *J. Geophys. Res. Oceans* **120**: 7329–7345. doi:10.1002/2015JC010885
- Sarhan, T., J. García Lafuente, M. Vargas, J. M. Vargas, and F. Plaza. 2000. Upwelling mechanisms in the northwestern Alboran Sea. *J. Mar. Syst.* **23**: 317–331. doi:10.1016/S0924-7963(99)00068-8
- Sotillo, M. G., and others. 2015. The MyOcean IBI Ocean Forecast and Reanalysis Systems: Operational products and roadmap to the future Copernicus Service. *J. Oper. Oceanogr.* **8**: 63–79. doi:10.1080/1755876X.2015.1014663
- Sotillo, M. G., and others. 2016. How is the surface Atlantic water inflow through the Gibraltar Strait forecasted? A Lagrangian validation of operational oceanographic services in the Alboran Sea and the Western Mediterranean. *Deep-Sea Res. Part II Top. Stud. Oceanogr.* **133**: 100–117. doi:10.1016/j.dsr2.2016.05.020
- Soto-Navarro, J., P. Lorente, E. Álvarez Fanjul, J. Carlos Sánchez-Garrido, and J. García-Lafuente. 2016. Surface circulation at the Strait of Gibraltar: A combined HF radar and high resolution model study. *J. Geophys. Res. Oceans* **121**: 2016–2034. doi:10.1002/2015JC011354
- Takeoka, H. 1984. Fundamental concepts of exchange and transport time scales in a coastal sea. *Cont. Shelf Res.* **3**: 311–326. doi:10.1016/0278-4343(84)90014-1
- Tartinville, B., E. Deleersnijder, and J. Rancher. 1997. The water residence time in the Mururoa atoll lagoon: Sensitivity analysis of a three-dimensional model. *Coral Reefs* **16**: 193–203. doi:10.1007/s003380050074
- Vargas-Yáñez, M., F. Plaza, J. García-Lafuente, T. Sarhan, J. M. Vargas, and P. Vélez-Belchi. 2002. About the seasonal variability of the Alboran Sea circulation. *J. Mar. Syst.* **35**: 229–248. doi:10.1016/S0924-7963(02)00128-8
- Viero, D. P., and A. Defina. 2016. Water age, exposure time, and local flushing time in semi-enclosed, tidal basins with negligible freshwater inflow. *J. Mar. Syst.* **156**: 16–29. doi:10.1016/j.jmarsys.2015.11.006
- Watson, G., and I. S. Robinson. 1990. A study of internal wave propagation in the Strait of Gibraltar using shore-based marine radar images. *J. Phys. Oceanogr.* **20**: 374–395. doi:10.1175/1520-0485(1990)020<0374:ASOIWP>2.0.CO;2
- Zimmerman, J. T. F. 1976. Mixing and flushing of tidal embayments in the western Dutch Wadden Sea part I: Distribution of salinity and calculation of mixing time scales. *Neth. J. Sea Res.* **10**: 149–191. doi:10.1016/0077-7579(76)90013-2

Acknowledgments

The notable involvement and collaboration of researchers from Puertos del Estado and Bay of Algeciras Port Authority is warmly recognized. Special thanks go to the crew of CEUTAMAR UNO and CEUTAMAR CINCO ships from the Bay of Algeciras Port Authority, who gave support during the field experiments. The model simulations have been run in the supercomputing centers of Puertos del Estado and the Supercomputing and Bioinnovation Center of the University of Malaga (PICASSO). Financial support from the Regional Government Junta de Andalucía through the Excellence Research Project MOCBASE (P12-RNM-1540) and from the Spanish Economy and Competitiveness Ministry through the Research Project ENCIBA (CTM2013-40886-P) are acknowledged. SS acknowledges financial support from the projects P12-RNM-1540. JCSG and CN acknowledge support from the project CTM2013-40886-P.

Conflict of Interest

None declared.

Submitted 27 July 2017

Revised 29 September 2017

Accepted 26 November 2017

Associate editor: Xiao Hua Wang